

Near-GeV Electron Beams at a Few Per-Mille Level from a Laser Wakefield Accelerator via Density-Tailored Plasma


L. T. Ke^{1,2}, K. Feng¹, W. T. Wang^{1,*}, Z. Y. Qin^{3,†}, C. H. Yu,³ Y. Wu,¹ Y. Chen,¹ R. Qi,¹ Z. J. Zhang,³ Y. Xu,¹ X. J. Yang,¹ Y. X. Leng,^{1,4} J. S. Liu,^{1,3,‡} R. X. Li,^{1,2,4,§} and Z. Z. Xu^{1,2,4}

¹State Key Laboratory of High Field Laser Physics and CAS Center for Excellence in Ultra-intense Laser Science, Shanghai Institute of Optics and Fine Mechanics (SIOM), Chinese Academy of Sciences (CAS), Shanghai 201800, China

²Center of Materials Science and Optoelectronics Engineering, University of Chinese Academy of Sciences, Beijing 100049, People's Republic of China

³Department of Physics, Shanghai Normal University, Shanghai 200234, People's Republic of China

⁴School of Physical Science and Technology, Shanghai Tech University, Shanghai 200031, People's Republic of China

 (Received 16 June 2020; revised 18 March 2021; accepted 28 April 2021; published 25 May 2021; corrected 8 July 2021)

A simple, efficient scheme was developed to obtain near-gigaelectronvolt electron beams with energy spreads of few per-mille level in a single-stage laser wakefield accelerator. Longitudinal plasma density was tailored to control relativistic laser-beam evolution, resulting in injection, dechirping, and a quasi-phase-stable acceleration. With this scheme, electron beams with peak energies of 780–840 MeV, rms energy spreads of 2.4%–4.1%, charges of 8.5–23.6 pC, and rms divergences of 0.1–0.4 mrad were experimentally obtained. Quasi-three-dimensional particle-in-cell simulations agreed well with the experimental results. The dechirping strength was estimated to reach up to 11 TeV/mm/m, which is higher than previously obtained results. Such high-quality electron beams will boost the development of compact intense coherent radiation sources and x-ray free-electron lasers.

DOI: [10.1103/PhysRevLett.126.214801](https://doi.org/10.1103/PhysRevLett.126.214801)

Plasma-based accelerators can accelerate electron beams (e beams) to the gigaelectronvolt (GeV) level within a few centimeters owing to their extremely high accelerating gradient [1–4]. Such high-energy e beams are typically produced by capillary-discharge waveguides [5,6] or long gas cells [7–9], and an energy level of 7.8 GeV has been achieved [10]. Although laser wakefield accelerators (LWFAs) can produce e beams with high energy, their energy spreads remain at a few percent level. This inherent problem hinders their potential applications in developing novel light sources [11–13] for which the energy spreads should be at a few per-mille level. Some theoretical schemes with an additional tailored escort e beam [14], tailored plasma profiles [15–17], or threshold-controlled ionization injections [18,19] have been proposed over recent years to reduce the energy spread down to the few per-mille or even millesimal level. These proposals, however, are experimentally challenging. In the experiments, the energy spread has been significantly reduced from 100% [20] to tens-of-percent levels [4] and from the few percent level [7,21,22] to the few per-mille level. Typically, per-mille-level e beams are realized by cascaded acceleration [23,24] wherein the injection and acceleration processes are separated and a minimum level of 4% has been achieved. However, this scheme requires a sophisticated configuration and is complicated. Hence, viable schemes to achieve the per-mille level are still unavailable and further research is required.

Recently, several types of dechirpers were proposed for e beams from linear accelerators [25–27] to reduce energy spreads from the percent level to the few per-mille level. The dechirping process utilizes a suitable field with a positive (negative) slope to reduce the negative (positive) chirp of an e beam. Similar processes are also applicable for LWFAs [17,28]. Generally, an injected beam with a negative chirp will rapidly undergo a chirp inversion owing to the positive-slope accelerating field, which is common in a blowout regime. Once the chirp reverses and becomes positive, the energy spread continues increasing. Therefore, the construction of an appropriate field and the method of interaction of the field with the e beam pose a challenge to effective dechirping.

The relativistic self-focusing of a laser is significant in laser-plasma interaction. Such self-focusing usually occurs when the power of a laser $P \gtrsim P_c$, where P_c is the critical power for self-focusing [29]. Self-focusing can be used to extend the acceleration distance and control the injection process [30]. When the relevant parameters are appropriately set, it is found that the defocusing can induce both chirp mitigation and quasi-phase-stable acceleration (QPSA) [31,32], implying that the accelerated e beam in an LWFA remains in a quasistable phase in a wakefield where the e beam witnesses an almost stable acceleration field. During the laser defocusing process, a sawtoothlike accelerating field is formed, leading to an interaction between a positive-chirped e beam and an accelerating

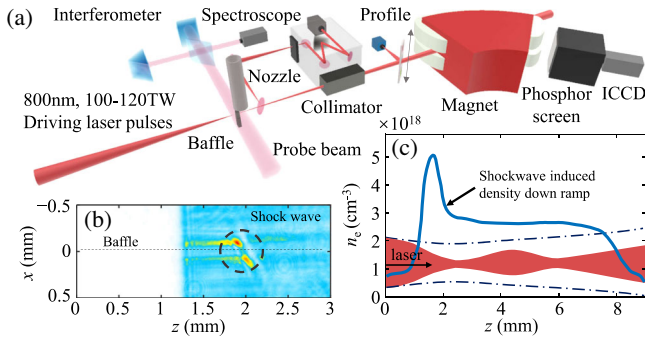


FIG. 1. Schematic of the experimental setup. (a) A perforated baffle was inserted upright into the flow of a supersonic gas nozzle. A 100–120 TW, 25-fs laser pulse polarized along the horizontal direction was focused onto the gas target and propagated through the hole of the baffle. The spectra of the generated electrons were measured with a 1.1-T magnetic spectrometer. (b) The shock wave in the shadow graph is circled with a dashed line. The optical axis is at zero. (c) The retrieved on-axis plasma density profile ranges from the center of the baffle. The evolution of the laser beam in vacuum (dashed line) and in the plasma (red shaded area) are also shown, respectively.

field with a negative slope. Thus, high-energy e beams with ultralow energy spreads can be generated.

In this Letter, we propose an efficient and viable scheme to achieve few per-mille level near-GeV e beams by using a tailored plasma density profile to guide the self-focusing process of the laser pulse. As a positive feedback, the focusing process controls the injection of electrons, and the defocusing process induces a QPSA and dechirping process. In the experiments, the generated e beams have peak energies of 780–840 MeV, root-mean-squared (rms) energy spreads of 2.4%–4.1%, charges of 8.5–23.6 pC, and rms divergences of 0.1–0.4 mrad. These e beams with high-quality characteristics may be applied in compact, intense, coherent LWFA-based free-electron lasers (FELs) and radiation sources.

The experiments were conducted using a 200-TW Ti:sapphire laser system with 1-Hz repetition rate based on chirped pulse amplification [33]. The setup is shown in Fig. 1(a). A laser pulse with 800-nm central wavelength was focused onto a gas target by an $f/30$ off-axis parabolic mirror. The vacuum focal spot sizes (w_{FWHM}) were measured to be $40 \pm 1 \mu\text{m}$ and $38 \pm 1 \mu\text{m}$ full width at half maximum (FWHM) in the vertical and horizontal directions, respectively (which for a Gaussian profile implies $1/e$ field profile radius $r_0 = w_{\text{FWHM}}/\sqrt{2\ln 2} \approx 34 \pm 1 \mu\text{m}$). The peak intensity was estimated as $2.9\text{--}3.6 \times 10^{18} \text{ W/cm}^2$, corresponding to a normalized amplitude $a_0 \approx 1.2\text{--}1.3$. The target assembly consisted of a perforated baffle and a pulsed helium gas valve connected to a nozzle with a bore diameter of 6 mm. By adjusting the relative distance between the baffle and the nozzle along the optical axis, a structured gas profile with a shock wave can be produced. The baffle was inserted in the upstream region of the supersonic flow to generate a density

down ramp. A probe beam split from the main laser pulse passed perpendicularly through the gas target and entered a Michelson-type interferometer using a $4f$ optical imaging system for measuring the shock wave and plasma density. The e beams were characterized by a 1.1-T magnet spectrometer, with which the energy spectrum, charge and divergence could be obtained. The energy spectrometer has an energy resolution of 0.2% at 780 MeV with 0.1 mrad divergence, and the uncertainty of the measured peak energy is 2% considering the pointing fluctuation of ± 0.6 mrad of the e beams.

In the experiments, the laser pulse was focused at the gas behind the baffle. A shock wave was formed at a distance less than the λ_{os} scale by adjusting the position of the baffle along the optical axis, as shown in Fig. 1(b), where λ_{os} is the oscillation period of the laser in a constant density plateau [34]. The e beams were expected to be injected into the bubble before the laser defocused. Figure 1(c) shows the constructed plasma density which peaks at $(5 \pm 0.5) \times 10^{18} \text{ cm}^{-3}$ and has a down ramp of $\sim 160 \mu\text{m}$. This can also be seen from the shock-wave shadow graph shown in Fig. 1(b). The down ramp is followed by a nearly 6-mm long $(2.6 \pm 0.5) \times 10^{18} \text{ cm}^{-3}$ density plateau. Figure 2(a) shows the spectra of the e beams achieved using these parameters. The e beams have peak energies of 780–840 MeV, rms energy spreads of 2.4%–4.1%, charges of 8.5–23.6 pC, and rms divergences of 0.1–0.4 mrad. The spatially integrated energy spectrum of the 13th shot shown in Fig. 2(b) indicates that the charge per energy interval was 1.5 pC/MeV. The average 6D brightness $B_{6D,n} = I/(e_n^2 \sigma_\delta)$, and it is defined as the peak current in the e beam core divided by the product of the rms transverse normalized emittances and the rms fractional energy in units of 0.1% [35]. In the calculation of $B_{6D,n}$, the transverse normalized emittance is estimated by $\epsilon_n = \gamma \sigma_x \sigma_\theta$, where γ is the relativistic Lorentz factor, and σ_x and σ_θ are the transverse size and the rms divergence of the e beam, respectively. Although e beam size σ_x and pulse duration at the exit of the LWFA are not measured, they are assumed to be $1.5 \mu\text{m}$ and 2 fs for an estimation [36–38]. The σ_θ and the σ_δ were set as 0.2 mrad and 0.3% with $\gamma = 1600$ and a charge of 16 pC. By using the aforementioned parameters, $B_{6D,n}$ was estimated as $\sim 10^{16} \text{ A/m}^2/0.1\%$. The beam properties, including the charge, energy spread, and even chirp degree can be controlled by manipulating the focal location and plasma density [34]. The average accelerating field was estimated as $\sim 142 \text{ GV/m}$ by assuming an accelerating length of 5.8 mm (according to the following simulation results). As the density transition used in this scheme is insufficient for the expansion of the bubble to capture the e beam from the second bubble into the first bubble at the density down ramp, the cascaded acceleration was excluded. In addition, only one e beam was detected on the scintillating screen for each shot, which excludes the beam driven acceleration. Thus, a QPSA stage in the first bubble is essential for achieving high energy in such a short distance.

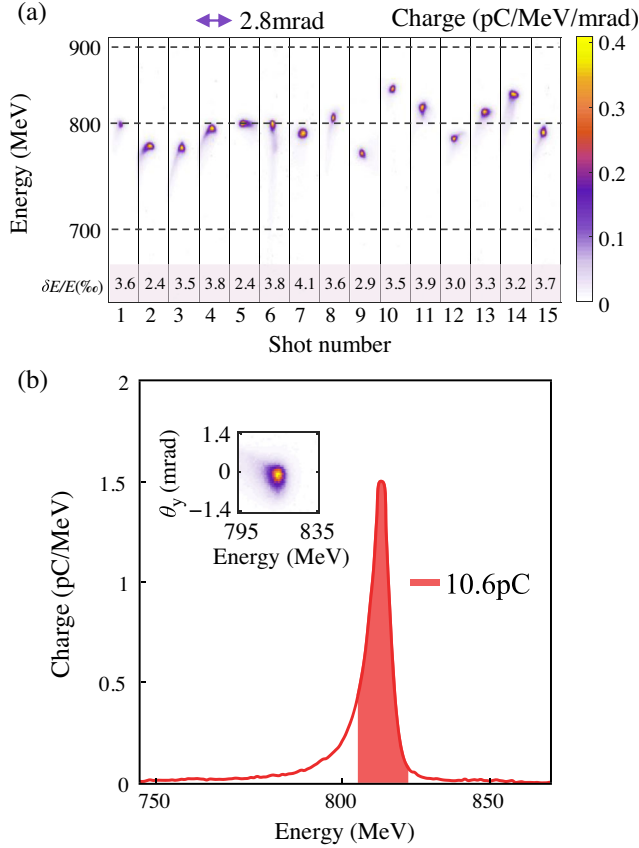


FIG. 2. Measured e beams energy spectra. (a) The raw energy spectra of 15 shots with energy spreads ranging from 2.4%–4.1%. The color map represents the charge density (pC/MeV/mrad) on the detector. (b) The spatially integrated energy spectrum of the 13th shot in (a). The peak energy of this shot is 817 MeV, and the rms relative energy spread is 3.3%. The filled area represents the charge of the beam corresponding to 10.6 pC within a threefold relative energy spread. The inset shows a magnification of shot 13 rotated 90° clockwise. The rms divergence is 0.25 mrad.

To further explore the underlying physics behind the generation of near-GeV e beams with ultralow energy spreads, quasi-three-dimensional particle-in-cell simulations were performed with Fourier-Bessel particle-in-cell (FBPIC) code [39,40]. The parameters used in the simulations matched the experimental conditions. The longitudinal and transverse window sizes were 50 and 120 μm , respectively. The grid cell size was determined as $\Delta z = 0.04 \mu\text{m}$ and $\Delta r = 0.12 \mu\text{m}$, with 16 macroparticles per cell. A linearly polarized laser pulse with a wavelength $\lambda_0 = 0.8 \mu\text{m}$, a normalized amplitude $a_0 = 1.24$, a pulse duration $\tau = 25$ fs, and a focal spot radius $r_0 = 34 \mu\text{m}$ was launched from the left boundary of the simulation box along the z axis and focused at 1.4 mm behind the entrance of the plasma. The laser pulse was assumed to be described by a Gaussian function. The density profile used in simulations was close to the measured one in experiments, as shown by the black line in Fig. 3(a).

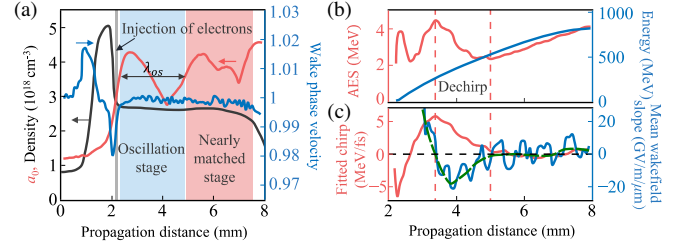


FIG. 3. Simulated evolution of various parameters. (a) Normalized vector potential (a_0), wake phase velocity (β_p), and plasma density. Here, β_p (blue line) is calculated at the rear of the bubble where the longitudinal electric field is zero. It reached the minimum near the end of the density down ramp. The evolution of a_0 (red line) can be separated as an oscillation period (blue shaded area) and a nearly matched period (red shaded area). (b), (c) The absolute energy spread (AES; red line) has a maximum of 4.5 MeV corresponding to a relative energy spread (RES) of 1.7% and a minimum of 2.4 MeV corresponding to an RES of 4.6%. The red dashed lines indicate the locations where the dechirping process started and completed. The green dashed line shows the fitted of the mean longitudinal wakefield slope (MLWS).

The density up ramp at the entrance of the plasma offered an appropriate distance for laser evolution. Electrons were not injected into the bubble throughout the density up ramp. As the laser entered the density down ramp, the bubble expanded, and the wake phase velocity β_p at the rear of the bubble reduced considerably. These changes were caused by an increase in a_0 and a decrease in plasma density. The injection was triggered near the end of the density down ramp, as indicated by the gray area in Fig. 3(a) because of the synergistic function of the density down ramp and the self-focusing of the laser. Hence, the injection is termed synergistic injection. In both the experiments and simulations, the injection ceased when the focal location was shifted forward (in the propagation direction) or backward from the density peak by more than 1 mm [34]. The reduction in charge was due to the decrease in a_0 and a'_0 , which is the derivative of a_0 with respect to the propagation distance, at the injection point [34], indicating that the self-focusing in our scheme plays an important role in realizing localized injections [22,30,41]. The influence of down ramp width L_{ramp} was also investigated, which showed that a larger or smaller L_{ramp} would lead to a reduced injected charge. Thus, the results show that both the density down ramp and the laser self-focusing contributed to the occurrence of injection in our scheme [34].

Figure 3(b) shows the evolution of the energy and AES of the e beam. The corresponding fitted chirp and MLWS over the length of the e beam are shown in Fig. 3(c). Chirp evolution was dominated by the MLWS. As a_0 decreased after injection, the positive MLWS became negative and the chirp of the e beam was compensated gradually. Under optimized conditions, the chirp was fully removed, and the corresponding AES decreased from 4.5 to 2.4 MeV [Fig. 3(b)]. After that, the chirp remained approximately

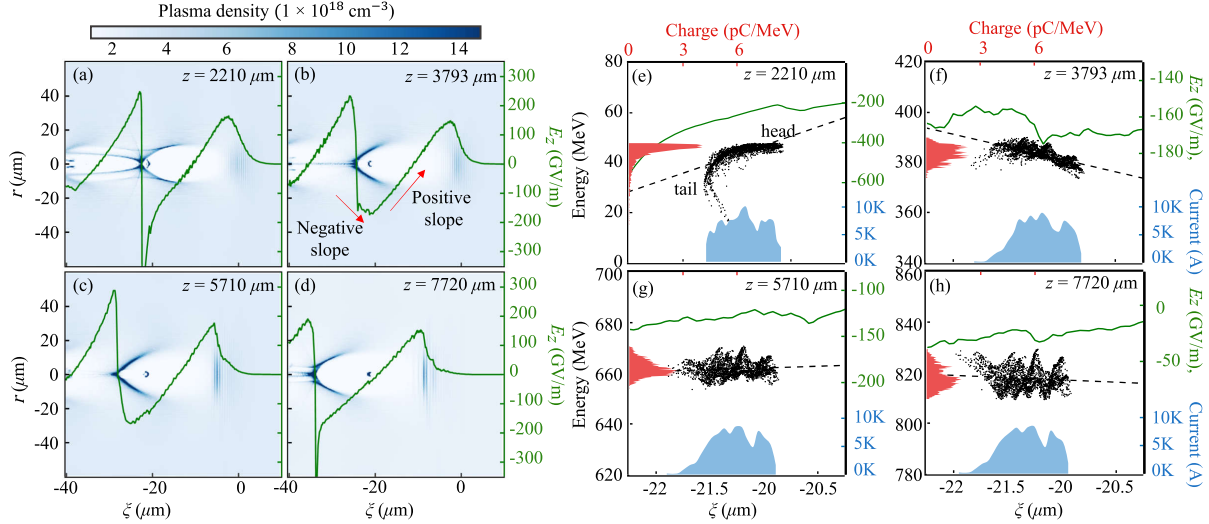


FIG. 4. Snapshots of electron density distribution in $r - \xi$ plane, where $\xi = z - ct$, the on-axis plasma field lineouts (green line), and the phase space dynamics of the e beam at different distances in the PIC simulation. (a) The e beam resides in a highly nonlinear accelerating field just after injection. (b) As the laser defocuses, the electron density at the rear of the bubble decreases. A sawtoothlike accelerating field with a gradual negative slope is formed. (c) The beam-loading effect helps sustain the relative energy spread during the final acceleration process. (d) The e beam approaches dephasing. (e)–(h) The corresponding phase space dynamics and the localized longitudinal wakefield of the e beams for (a)–(d). The dashed line represents the fitted chirp of the e beam. The electron spectra (red shaded area) and the current profile (blue shaded area) of the entire e beam are also shown.

zero during the subsequent acceleration. The process is described in detail as in the next paragraph.

When the density down ramp terminated, β_p increased, and injection ceased. The chirp of the e beam that had just been injected into the bubble was negative as the head of the beam was injected earlier and gained much more energy than the tail. Since the slope of the accelerating field was positive, the trailing electrons experienced a higher longitudinal accelerating field than the front [Figs. 4(a) and 4(e)]. Consequently, the chirp reversed rapidly after an accelerating length of hundreds of micrometers, as shown in Figs. 3(c) and 4(f). When the laser intensity decreased from the maximum, the density singularity at the rear of the bubble abated, creating a sawtoothlike accelerating field [Fig. 4(b)]. At this position, the estimated chirp was 4.7 MeV/fs [Fig. 3(c)] [28]. Owing to the transformation of the accelerating field during the dechirping process, the e beam with the positive chirp gradually slipped back to the rear of the bubble during transition from the accelerating field with a positive slope to one with a slightly negative slope [Fig. 4(f)]. Although the entire beam remained in the accelerating phase, the trailing electrons witnessed a weaker accelerating field. Thus, the chirp was compensated and decreased to 0.4 MeV/fs after about $\lambda_{os}/2$ [Fig. 3(c)] indicating a dechirping strength of 11 TeV/mm/m [26]. The total energy spread of the e beam after dechirping was almost equal to the slice energy spread. With increasing energy gain, the e beam moved away from the rear of the bubble and reverted to the accelerating field with the positive slope. The beam-loading effect was clearly observed at this point. Each part of the e

beam witnessed almost the same acceleration gradient as shown in Figs. 4(c) and 4(g). The subsequent increase in the AES after reaching the minimum (over the complete accelerating process, to be precise), was due to betatron slippage [42] and betatron-motion-induced transverse dependence of the accelerating fields [43]. Finally, an e beam with a peak energy of 817 MeV, a charge of 16.6 pC and an rms energy spread of 5% was achieved [Figs. 4(d) and 4(h)], and it agreed well with the experimental results. Further simulations showed that the key to the generation of a small final RES is the matching between the initial chirp and the dechirping process. If the dechirping process did not match the initial chirp, even a small initial chirp would lead to a large energy spread at the percent level [34]. Simulations with higher spatial resolution were performed to ensure convergence.

In conclusion, we proposed and experimentally demonstrated a feasible scheme to achieve near-GeV e beams with few per-mille RES based on the tailored plasma density profiles. The simulation results agreed with the experimental results. Further, the simulations showed that laser evolution controls the complete laser-plasma interaction process, including the injection and the dechirping process. Matched dechirping can induce a reduction in the RES by a factor of 3 and the total energy spread of the e beams can be approximated as the slice energy spread. We believe these e beams will promote advances in the field of tabletop x-ray FELs and stable x-ray and gamma ray sources in the future.

This work was supported by the National Natural Science Foundation of China (Grants No. 11127901,

No. 11875065, No. 11974251, and No. 11991072), the Natural Science Foundation of Shanghai (No. 18JC1414800 and No. 18ZR1444500), Strategic Priority Research Program (B) (Grant No. XDB16), the State Key Laboratory Program of Chinese Ministry of Science and Technology, and the financial support from Youth Innovation Promotion Association, CAS (Y201952).

L. K. and K. F. contributed equally to this work.

* wwt1980@siom.ac.cn
 † phyzyqin@shnu.edu.cn
 ‡ michaeljs_liu@siom.ac.cn
 § ruxinli@mail.shnc.ac.cn

- [1] T. Tajima and J. M. Dawson, Laser Electron Accelerator, *Phys. Rev. Lett.* **43**, 267 (1979).
- [2] S. P. Mangles, C. D. Murphy, Z. Najmudin, A. G. Thomas, J. L. Collier, A. E. Dangor *et al.*, Monoenergetic beams of relativistic electrons from intense laser-plasma interactions, *Nature (London)* **431**, 535 (2004).
- [3] C. G. Geddes, C. S. Toth, J. Van Tilborg, E. Esarey, C. B. Schroeder, D. Bruhwiler, C. Nieter, J. Cary, and W. P. Leemans, High-quality electron beams from a laser wakefield accelerator using plasma-channel guiding, *Nature (London)* **431**, 538 (2004).
- [4] J. Faure, Y. Glinec, A. Pukhov, S. Kiselev, S. Gordienko, E. Lefebvre, J.-P. Rousseau, F. Burgy, and V. Malka, A laser-plasma accelerator producing monoenergetic electron beams, *Nature (London)* **431**, 541 (2004).
- [5] S. Karsch, J. Osterhoff, A. Popp, T. P. Rowlands-Rees, Z. Major, M. Fuchs *et al.*, GeV-scale electron acceleration in a gas-filled capillary discharge waveguide, *New J. Phys.* **9**, 415 (2007).
- [6] W. P. Leemans, B. Nagler, A. J. Gonsalves, C. Tóth, K. Nakamura, C. G. R. Geddes, E. Esarey, C. B. Schroeder, and S. M. Hooker, GeV electron beams from a centimeter-scale accelerator, *Nat. Phys.* **2**, 696 (2006).
- [7] X. M. Wang, R. Zgadzaj, N. Fazel, Z. Y. Li, S. A. Yi, X. Zhang *et al.*, Quasi-monoenergetic laser-plasma acceleration of electrons to 2 GeV, *Nat. Commun.* **4**, 1988 (2013).
- [8] J. Osterhoff, A. Popp, Z. Major, B. Marx, T. P. Rowlands-Rees, M. Fuchs *et al.*, Generation of Stable, Low-Divergence Electron Beams by Laser-Wakefield Acceleration in a Steady-State-Flow Gas Cell, *Phys. Rev. Lett.* **101**, 085002 (2008).
- [9] C. E. Clayton, J. E. Ralph, F. Albert, R. A. Fonseca, S. H. Glenzer, C. Joshi *et al.*, Self-Guided Laser Wakefield Acceleration beyond 1 GeV Using Ionization-Induced Injection, *Phys. Rev. Lett.* **105**, 105003 (2010).
- [10] A. J. Gonsalves, K. Nakamura, J. Daniels, C. Benedetti, C. Pieronek, T. C. H. de Raadt *et al.*, Petawatt Laser Guiding and Electron Beam Acceleration to 8 GeV in a Laser-Heated Capillary Discharge Waveguide, *Phys. Rev. Lett.* **122**, 084801 (2019).
- [11] A. R. Maier, A. Meseck, S. Reiche, C. B. Schroeder, T. Seggebrock, and F. Grüner, Demonstration Scheme for a Laser-Plasma-Driven Free-Electron Laser, *Phys. Rev. X* **2**, 031019 (2012).
- [12] Z. R. Huang, Y. T. Ding, and C. B. Schroeder, Compact X-Ray Free-Electron Laser from a Laser-Plasma Accelerator using a Transverse-Gradient Undulator, *Phys. Rev. Lett.* **109**, 204801 (2012).
- [13] S. Corde, K. Ta Phuoc, G. Lambert, R. Fitour, V. Malka, A. Rousse, A. Beck, and E. Lefebvre, Femtosecond x rays from laser-plasma accelerators, *Rev. Mod. Phys.* **85**, 1 (2013).
- [14] G. G. Manahan, A. F. Habib, P. Scherkl, P. Delinikolas, A. Beaton, A. Knetsch *et al.*, Single-stage plasma-based correlated energy spread compensation for ultrahigh 6D brightness electron beams, *Nat. Commun.* **8**, 15705 (2017).
- [15] Z. J. Zhang, W. T. Li, J. S. Liu, W. T. Wang, C. H. Yu, Y. Tian *et al.*, Energy spread minimization in a cascaded laser wakefield accelerator via velocity bunching, *Phys. Plasmas* **23**, 053106 (2016).
- [16] X. L. Xu, F. Li, W. An, T. N. Dalichaouch, P. Yu, W. Lu, C. Joshi, and W. B. Mori, High quality electron bunch generation using a longitudinal density-tailored plasma-based accelerator in the three-dimensional blowout regime, *Phys. Rev. ST Accel. Beams* **20**, 111303 (2017).
- [17] R. Brinkmann, N. Delbos, I. Dornmair, M. Kirchen, R. Assmann, C. Behrens *et al.*, Chirp Mitigation of Plasma-Accelerated Beams by a Modulated Plasma Density, *Phys. Rev. Lett.* **118**, 214801 (2017).
- [18] P. Tomassini, D. Terzani, F. Baffigi, F. Brandi, L. Fulgentini, P. Koester, L. Labate, D. Palla, and L. A. Gizzi, High-quality 5 GeV electron bunches with resonant multi-pulse ionization injection, *Plasma Phys. Controlled Fusion* **62**, 014010 (2020).
- [19] X. L. Xu, C. H. Pai, C. J. Zhang, F. Li, Y. Wan, Y. P. Wu *et al.*, Nanoscale Electron Bunching in Laser-Triggered Ionization Injection in Plasma Accelerators, *Phys. Rev. Lett.* **117**, 034801 (2016).
- [20] V. Malka, S. Fritzler, E. Lefebvre, M.-M. Aleonard, F. Burgy, J.-P. Chambaret *et al.*, Electron acceleration by a wake field forced by an intense ultrashort laser pulse, *Science* **298**, 1596 (2002).
- [21] J. Faure, C. Rechatin, A. Norlin, A. Lifschitz, Y. Glinec, and V. Malka, Controlled injection and acceleration of electrons in plasma wakefields by colliding laser pulses, *Nature (London)* **444**, 737 (2006).
- [22] A. Buck, J. Wenz, J. Xu, K. Khrennikov, K. Schmid, M. Heigoldt *et al.*, Shock-Front Injector for High-Quality Laser-Plasma Acceleration, *Phys. Rev. Lett.* **110**, 185006 (2013).
- [23] J. S. Liu, C. Q. Xia, W. T. Wang, H. Y. Lu, C. Wang, A. H. Deng *et al.*, All-Optical Cascaded Laser Wakefield Accelerator Using Ionization-Induced Injection, *Phys. Rev. Lett.* **107**, 035001 (2011).
- [24] W. T. Wang, W. T. Li, J. S. Liu, Z. J. Zhang, R. Qi, C. H. Yu *et al.*, High-Brightness High-Energy Electron Beams from a Laser Wakefield Accelerator via Energy Chirp Control, *Phys. Rev. Lett.* **117**, 124801 (2016).
- [25] Y. P. Wu, J. F. Hua, Z. Zhou, J. Zhang, S. Liu, B. Peng *et al.*, Phase Space Dynamics of a Plasma Wakefield Dechirper for Energy Spread Reduction, *Phys. Rev. Lett.* **122**, 204804 (2019).
- [26] R. D'Arcy, S. Wesch, A. Aschikhin, S. Bohlen, C. Behrens, M. J. Garland *et al.*, Tunable Plasma-Based Energy Dechirper, *Phys. Rev. Lett.* **122**, 034801 (2019).

- [27] P. Emma, M. Venturini, K. L. Bane, G. Stupakov, H. S. Kang, M. S. Chae *et al.*, Experimental Demonstration of Energy-Chirp Control in Relativistic Electron Bunches Using a Corrugated Pipe, *Phys. Rev. Lett.* **112**, 034801 (2014).
- [28] A. Dopp, C. Thauray, E. Guillaume, F. Massimo, A. Lifschitz, I. Andriyash, J.-P. Goddet, A. Tazfi, K. Ta Phuoc, and V. Malka, Energy-Chirp Compensation in a Laser Wakefield Accelerator, *Phys. Rev. Lett.* **121**, 074802 (2018).
- [29] P. Sprangle, C. Tang, and E. Esarey, Relativistic self-focusing of short-pulse radiation beams in plasmas, *IEEE Trans. Plasma Sci.* **15**, 145 (1987).
- [30] A. J. Gonsalves, K. Nakamura, C. Lin, D. Panasenkov, S. Shiraishi, T. Sokollik *et al.*, Tunable laser plasma accelerator based on longitudinal density tailoring, *Nat. Phys.* **7**, 862 (2011).
- [31] W. Li, J. Liu, W. Wang, Z. Zhang, Q. Chen, Y. Tian *et al.*, The phase-lock dynamics of the laser wakefield acceleration with an intensity-decaying laser pulse, *Appl. Phys. Lett.* **104**, 093510 (2014).
- [32] W. Rittershofer, C. B. Schroeder, E. Esarey, F. J. Grüner, and W. P. Leemans, Tapered plasma channels to phase-lock accelerating and focusing forces in laser-plasma accelerators, *Phys. Plasmas* **17**, 063104 (2010).
- [33] F. X. Wu, Z. X. Zhang, X. J. Yang, J. B. Hu, P. H. Ji, J. Y. Gui *et al.*, Performance improvement of a 200 TW/1 Hz Ti:sapphire laser for laser wakefield electron accelerator, *Opt. Laser Technol.* **131**, 106453 (2020).
- [34] See Supplemental Material at <http://link.aps.org/supplemental/10.1103/PhysRevLett.126.214801> for estimation of λ_{os} ; for the discussion about the controlling of beam properties, which includes Ref. [29]; for a demonstration of synergistic injection; for the relation between the initial chirp and dechirping.
- [35] S. Di Mitri and M. Cornacchia, Electron beam brightness in linac drivers for free-electron-lasers, *Phys. Rep.* **539**, 1 (2014).
- [36] O. Lundh, J. Lim, C. Rechatin, L. Ammoura, A. Ben-Ismaïl, X. Davoine *et al.*, Few femtosecond, few kiloampere electron bunch produced by a laser-plasma accelerator, *Nat. Phys.* **7**, 219 (2011).
- [37] K. Ta Phuoc, S. Corde, C. Thauray, V. Malka, A. Tazfi, J. P. Goddet, R. C. Shah, S. Sebban, and A. Rousse, All-optical Compton gamma-ray source, *Nat. Photonics* **6**, 308 (2012).
- [38] A. Buck, M. Nicolai, K. Schmid, C. M. S. Sears, A. Sävert, J. M. Mikhailova, F. Krausz, M. C. Kaluza, and L. Veisz, Real-time observation of laser-driven electron acceleration, *Nat. Phys.* **7**, 543 (2011).
- [39] R. Lehe, M. Kirchen, I. A. Andriyash, B. B. Godfrey, and J.-L. Vay, A spectral, quasi-cylindrical and dispersion-free particle-in-cell algorithm, *Comput. Phys. Commun.* **203**, 66 (2016).
- [40] S. Jalas, I. Dornmair, R. Lehe, H. Vincenti, J. L. Vay, M. Kirchen, and A. R. Maier, Accurate modeling of plasma acceleration with arbitrary order pseudo-spectral particle-in-cell methods, *Phys. Plasmas* **24**, 033115 (2017).
- [41] H.-E. Tsai, K. K. Swanson, S. K. Barber, R. Lehe, H.-S. Mao, D. E. Mittelberger *et al.*, Control of quasi-monoenergetic electron beams from laser-plasma accelerators with adjustable shock density profile, *Phys. Plasmas* **25**, 043107 (2018).
- [42] A. Ferran Pousa, A. Martinez de la Ossa, and R. W. Assmann, Intrinsic energy spread and bunch length growth in plasma-based accelerators due to betatron motion, *Sci. Rep.* **9**, 17690 (2019).
- [43] X. K. Li, P. A. P. Nghiem, and A. Mosnier, Toward low energy spread in plasma accelerators in quasilinear regime, *Phys. Rev. ST Accel. Beams* **21**, 111301 (2018).

Correction: An inline equation appearing in the fourth sentence of the seventh paragraph contained an error and has been fixed.